

PCCP

Accepted Manuscript



This is an *Accepted Manuscript*, which has been through the Royal Society of Chemistry peer review process and has been accepted for publication.

Accepted Manuscripts are published online shortly after acceptance, before technical editing, formatting and proof reading. Using this free service, authors can make their results available to the community, in citable form, before we publish the edited article. We will replace this *Accepted Manuscript* with the edited and formatted *Advance Article* as soon as it is available.

You can find more information about *Accepted Manuscripts* in the [Information for Authors](#).

Please note that technical editing may introduce minor changes to the text and/or graphics, which may alter content. The journal's standard [Terms & Conditions](#) and the [Ethical guidelines](#) still apply. In no event shall the Royal Society of Chemistry be held responsible for any errors or omissions in this *Accepted Manuscript* or any consequences arising from the use of any information it contains.



Vertical Heterostructure of MoS₂ and Graphene Nanoribbons by Two-Step Chemical Vapor Deposition for High-Gain Photodetectors

Rozan Mohamad Yunus,^a Hiroko Endo,^b Masaharu Tsuji^{a,b} and Hiroki Ago^{*,a,b,c}

Received 00th January 20xx,
Accepted 00th January 20xx

DOI: 10.1039/x0xx00000x

www.rsc.org/

Heterostructures of two-dimensional (2D) layered materials have attracted growing interest due to their unique properties and possible applications in electronics, photonics, and energy. Reduction of the dimensionality from 2D to one-dimensional (1D), such as graphene nanoribbons (GNRs), is also interesting due to the electron confinement effect and unique edge effects. Here, we demonstrate a bottom-up approach to grow vertical heterostructures of MoS₂ and GNRs by two-step chemical vapor deposition (CVD) method. Single-layer GNRs were first grown by ambient pressure CVD on an epitaxial Cu(100) film, followed by the second CVD process to grow MoS₂ over the GNRs. The MoS₂ layer was found to grow preferentially on the GNRs surface, while the coverage could be further tuned by adjusting the growth conditions. The MoS₂/GNR nanostructures show clear photosensitivity to visible light with an optical response much higher than that of a 2D MoS₂/graphene heterostructure. The ability to grow the novel 1D heterostructure of layered materials by a bottom-up CVD approach will open up a new avenue to expand the dimensionality of the material synthesis and applications.

Introduction

Recently, atomic sheets of two-dimensional (2D) layered materials, such as graphene,^{1,2} transition metal dichalcogenides (TMDCs),^{3,4} boron nitride,⁵ and phosphorene,⁶ have attracted a great interest due to their unique and excellent properties, and potential applications. The integration of these 2D materials is interesting, because new and unique functionalities are expected based on different constitutions with a variety of electronic and optical properties.⁷ Moreover, the heterostructures of atom-thick 2D materials offer optical transparency, mechanical flexibility, and promising transport properties for realizing electronic and photonic applications.

Single-layer graphene is a zero gap semiconductor and, thus graphene field-effect transistor (FET) shows low on/off ratios, but with extraordinary high carrier mobility (10,000 cm²/Vs).⁸ On the other hand, single-layer molybdenum disulfide (MoS₂) is a direct gap semiconductor with a wide band gap (1.9 eV),⁹ allowing to produce high on/off ratio FETs but with moderate mobility (typically 1~10 cm²/Vs).¹⁰ Hence, it is likely that in heterostructures of graphene and MoS₂, both materials can have valuable combination for future electronic devices. The heterostructures of MoS₂ and graphene have been applied to high gain photodetectors, photoresponsive memory

devices, and gate-tunable photocurrent generators.^{11–13} In addition, development of integrated circuits and nonvolatile memories were also demonstrated.^{13,14} However, most of these devices were made by using multiple transfer techniques to place single-layer graphene (MoS₂) on top of single-layer or multi-layer MoS₂ (graphene). The drawback of this multiple transfer is the possibility of contamination at the interface and difficulty in controlling the size as well as fabricating large devices.

Reducing the dimensionality of the 2D layered materials into 1D nanostructure is also an interesting approach to bring out new functionalities and phenomena. 1D structure of graphene, so-called graphene nanoribbons (GNRs) is a well-known material that shows unique electronic structures in which the band gap varies with the width, enabling the opening gap in graphene.^{15–18} In addition, unique spin-transport is expected for zigzag edge GNRs.¹⁹ Theoretical studies of MoS₂ nanoribbons also proposed unusual electronic structures with high stability and edge-dependent ferromagnetism.²⁰ Therefore, not only 2D heterostructure but also the 1D heterostructure is an interesting topic. However, as far as we know, there has been no attempt to synthesize 1D heterostructures, due to the difficulties in making such structures by mechanical exfoliation, which is widely used to prepare heterostack devices.

Here, we present an original approach to synthesize MoS₂/GNR heterostructures by a two-step chemical vapor deposition (CVD) method. After growing GNRs on an epitaxial Cu film by the first CVD step, the second CVD step was performed for the transferred GNRs to grow MoS₂. We succeeded to grow a new type of MoS₂/GNR heterostructure with different coverages depending on the CVD growth conditions. This was a unique growth process because 2D materials of MoS₂ could grow in 1D direction by following the 1D nature of our GNRs. The heterostructures were characterized by

^a Interdisciplinary Graduate School of Engineering Sciences, Kyushu University, Fukuoka 816-8580, Japan.

^b Institute for Materials Chemistry and Engineering (IMCE), Kyushu University, Fukuoka 816-8580, Japan.

^c PRESTO, Japan Science and Technology (JST), Saitama 332-0012, Japan.

*Email: ago@cm.kyushu-u.ac.jp

†Electronic Supplementary Information (ESI) available: Experimental methods, SEM images obtained by different growth conditions, TEM-EDX data, and PL spectra of MoS₂ grown on GNR and sapphire substrates. See DOI: 10.1039/x0xx00000x

different methods, scanning electron microscope (SEM), atomic force microscope (AFM), transmission electron microscope (TEM), Raman and photoluminescence (PL) spectroscopies. Furthermore, high photoinduced current modulation was observed using our MoS₂-GNR heterostructures upon illumination with visible light.

Experimental

Scheme 1 shows our two-step CVD processes carried out to synthesize the MoS₂/GNR heterostructure, and successive device fabrication and measurement. In the first step, single-layer GNRs were synthesized by ambient-pressure CVD at 975 °C on a heteroepitaxial Cu(100) film (Scheme 1a,b), as we reported previously.²¹ After transferring the GNRs on a SiO₂ (300 nm)/Si substrate by using poly(methyl methacrylate) (PMMA) and Cu etching solution (Scheme 1c),²¹ MoS₂ was directly grown using GNRs as a template by a second CVD process using MoO₃ and S feedstock (Scheme 1d). Detailed experimental methods as well as the CVD setup are described in Electronic Supplementary Information, ESI (Fig. S1). Scheme 1e illustrates the MoS₂/GNR heterostructure back-gated-FET fabricated by electron-beam (EB) lithography, metal deposition, and lift-off processes. Finally, the electronic properties of the FET devices were measured in dark and under illumination by visible light (Scheme 1f).

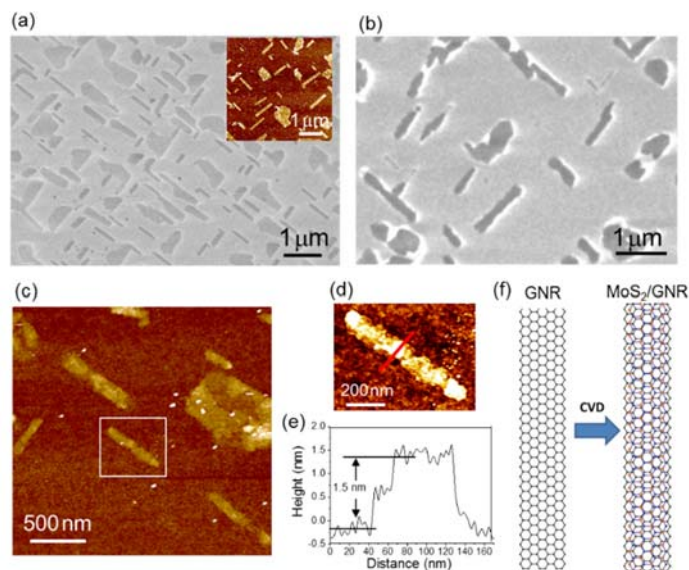
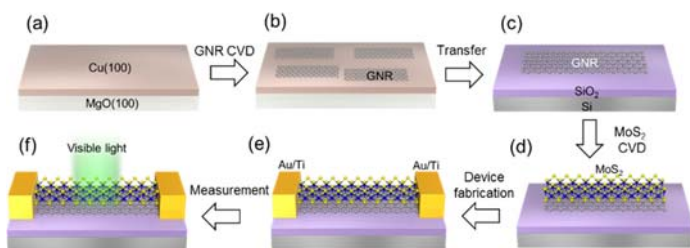


Fig. 1 (a) SEM and AFM (inset) images of transferred GNRs on SiO₂. (b,c) SEM and AFM images of the MoS₂/GNR heterostructures obtained after the MoS₂ CVD on the GNR/SiO₂ substrate. (d) Enlarged AFM image of one of MoS₂/GNRs, which is marked by white square in (c). (e) Height profile of the MoS₂/GNR measured along the red line in (d). (f) A schematic diagram of MoS₂ growth on GNR by the second CVD.

Then, we performed the second CVD to grow MoS₂ on this GNR/SiO₂/Si substrate using MoO₃ and S powder as feedstock. Fig. 1b shows SEM image after the second CVD at 900 °C for 30 min, where the dark contrast corresponds to the CVD-grown MoS₂. Interestingly, we found that MoS₂ selectively grows on the GNR surface while almost no MoS₂ domains are seen on the SiO₂ surface. In addition, most of the GNRs are fully covered with MoS₂. On the other hand, by controlling the CVD condition, we can synthesize the heterostructures with different MoS₂ coverage as illustrated in ESI (Fig. S2). Although several papers have reported the CVD growth of TMDCs on graphene made by mechanical exfoliation and CVD,^{11–14,22–25} this is the first time to grow TMDC over one-dimensional graphene nanoribbons. In other words, we succeeded in confining the 2D TMDC material into a 1D structure by using GNRs as a template, as illustrated in Fig. 1f. The particular reason for the selective growth on GNRs is not clear, but it is likely that surface adsorbed intermediate species tend to migrate on SiO₂ surface, while MoS₂ nucleation occurs on graphene lattice, due to van der Waals interaction. The strong interaction between Mo and C might be another reason for the selective growth. The selective growth reported here demonstrates that graphene lattice is a suitable platform for the growth of TMDCs compared with SiO₂ surface.

The AFM images also confirmed the preferential growth of MoS₂ on our GNRs (Fig. 1c,d); the GNR height becomes higher (from 0.7 nm to 1.5 nm) after the second CVD due to the growth of single-layer MoS₂ on top of the GNR (see Fig. 1e), while no MoS₂ domains were seen on the SiO₂ surface. As the heights of both single-layer graphene and MoS₂ measured by AFM are 0.7–0.8 nm, the measured height of the heterostructure (1.5 nm)



Scheme 1. Synthesis, fabrication, and device measurement processes of the vertical MoS₂/GNR heterostructure. (a,b) Oriented GNRs were grown on epitaxial Cu(100)/MgO(100) substrate by the first CVD step. (c) Transfer of GNRs onto a SiO₂/Si substrate. (d) The second CVD step for the MoS₂ growth on GNR. (e) Device fabrication. (g) Transport measurement.

Results and discussion

Figure 1a shows the SEM and AFM images of pristine GNRs taken after transferring onto a SiO₂/Si substrate. The typical width and length of these GNRs measured by SEM are 50–100 nm and 1–1.5 μm, respectively, with typical aspect ratios of ~14.²¹ As will be shown later, these nanoribbons are made of single-layer graphene. Reflecting the crystallographic orientation of the Cu(100) catalyst, these GNRs are oriented in two directions. The face-centered cubic (fcc) plane of the Cu(100) lattice guides the growth of GNRs along both [011]_{Cu} and [01-1]_{Cu} directions.²¹ As we reported previously, our low energy electron microscope (LEEM) analysis indicated that GNRs grown on Cu(100) film are single crystalline without grain boundaries.²¹

signifies the formation of single layer MoS₂ on GNR. TEM and energy dispersive x-ray (EDX) spectroscopy were also measured after transferring the MoS₂/GNRs from SiO₂ to a TEM grid. As presented in ESI (Fig. S3), the nanoribbon structure with the presence of MoS₂ was also confirmed by the TEM-EDX measurements.

Growth of MoS₂/GNR heterostructure was sensitive to the CVD conditions, such as the temperatures of MoO₃ and GNRs substrates as well as the distance between precursor and substrate. The surface coverage of GNRs with MoS₂ can be reduced by either decreasing the MoO₃ temperature or placing the GNR substrate farther from the MoO₃ (ESI, Fig. S2). By controlling the CVD growth condition, we can also synthesize the heterostructure partly covered with MoS₂, as shown in Fig. 3a,b. Again, no MoS₂ is seen on the SiO₂ surface, signifying that the GNR acts as a good template for MoS₂ growth.

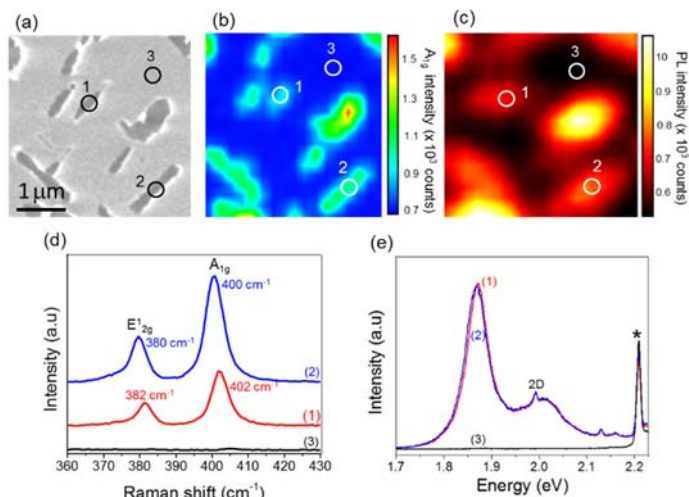


Fig. 2 SEM image (a) and corresponding Raman mapping images of the A_{1g} band intensity of MoS₂ (b) and the PL intensity (1.86 eV) from MoS₂ (c). Raman (d) and PL (e) spectra at the positions marked in (a-c).

Raman spectroscopy is a powerful and non-destructive means widely applied to graphene,^{26,27} and MoS₂^{28,29} to obtain intrinsic information, such as the number of layers, quality, and charged state. The Raman spectra measured at the positions 1, 2, and 3 marked in Figure 2a are shown in Figure 2d. Two characteristic Raman bands of MoS₂, originating in E_{12g} (in-plane vibration) and A_{1g} (out-of-plane vibration) modes,^{28,29} were clearly observed at the positions 1 and 2 but not at 3. The separation between A_{1g} and E_{12g} bands is known to correlate with the number of MoS₂ layers and it increases with increasing the number of MoS₂ layers.^{29–31} The separation between these two bands for our MoS₂-GNR heterostructures was 20 cm⁻¹ (see Fig. 2d), suggesting the growth of single-layer MoS₂. From the Raman mapping intensity of the A_{1g} band (Fig. 2b), it is clearly seen that the dark SEM contrast corresponds to MoS₂. We also measured photoluminescence (PL) from the MoS₂/GNR heterostructures (Figure 2c,e). Two prominent luminescence peaks were identified in the PL intensity spectrum (Fig. 2e) at 1.86 eV and 2.02 eV. The peak at 1.86 eV arising from the direct recombination of photo-generated electron-hole pairs, with the characteristic higher luminescence quantum efficiency of single-layer MoS₂, and the peak at 2.02 eV corresponds to the energy split of the valence band spin-orbital coupling of MoS₂ occurring in presence of the SiO₂/Si substrate.³² From the comparison with the single layer MoS₂ domains grown on sapphire (ESI, Fig. S4), we found that the PL intensity is reduced to ~1/6 when grown over the GNR due to quenching effect by GNRs.

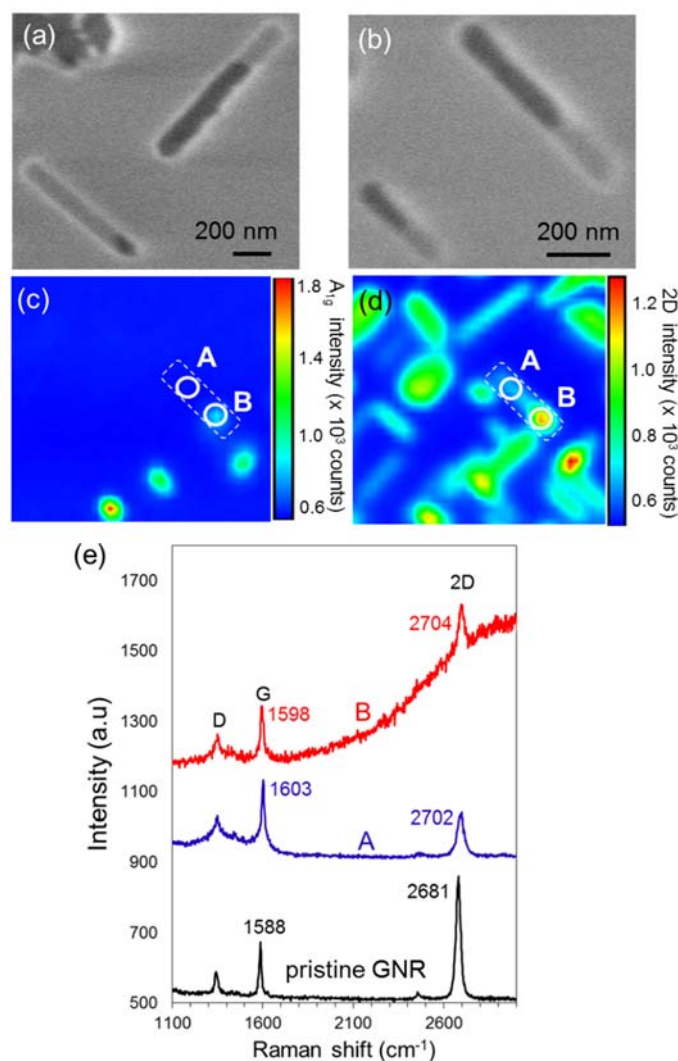


Fig. 3 Partially covered MoS₂/GNR heterostructures. (a,b) SEM images. MoS₂ A_{1g} (c) and GNR 2D (d) intensity mapping images of the same sample with (a) but measured at a different area. (e) Raman spectra measured at positions A and B marked in (c,d). For comparison, the Raman spectrum of a pristine GNR is also shown.

The Raman spectrum of the pristine GNR which was measured before the MoS₂ growth is shown in Figure 3e (black spectrum). The pristine GNR showed sharp G and 2D bands, and a narrow full width at half-maximum (FWHM) of 2D band, ~35 cm⁻¹, and I_{2D}/I_G is around 2, signifying that GNRs are single-layer. Because the

GNRs were synthesized by catalytic CVD over Cu(100) film, the defect-related D band was relatively weak ($I_D/I_G = 0.3$) in comparison to other GNRs produced by other top-down methods (top-down GNRs show $I_D/I_G > 1$).^{33–35} The Raman mapping images of MoS₂ A_{1g} and graphene 2D bands are shown in Fig. 3c and 3d, respectively, together with the corresponding Raman spectra (Fig. 3e).

Even after the MoS₂ CVD, the characteristic G and 2D bands of graphene were still observed, which suggests that the GNR structure is preserved during the MoS₂ growth (Fig. 3e, red and blue spectra). The uncovered area of the GNR showed reduced 2D band and enhanced D band which can be interpreted by slight damage to the graphene lattice as well as the thermally-enhanced interaction with the SiO₂ substrate as reported in the previous study.³⁶ The MoS₂-covered area (red spectrum) showed a strong background which originates in the luminescence from the overlying MoS₂, thus confirming the growth of MoS₂.

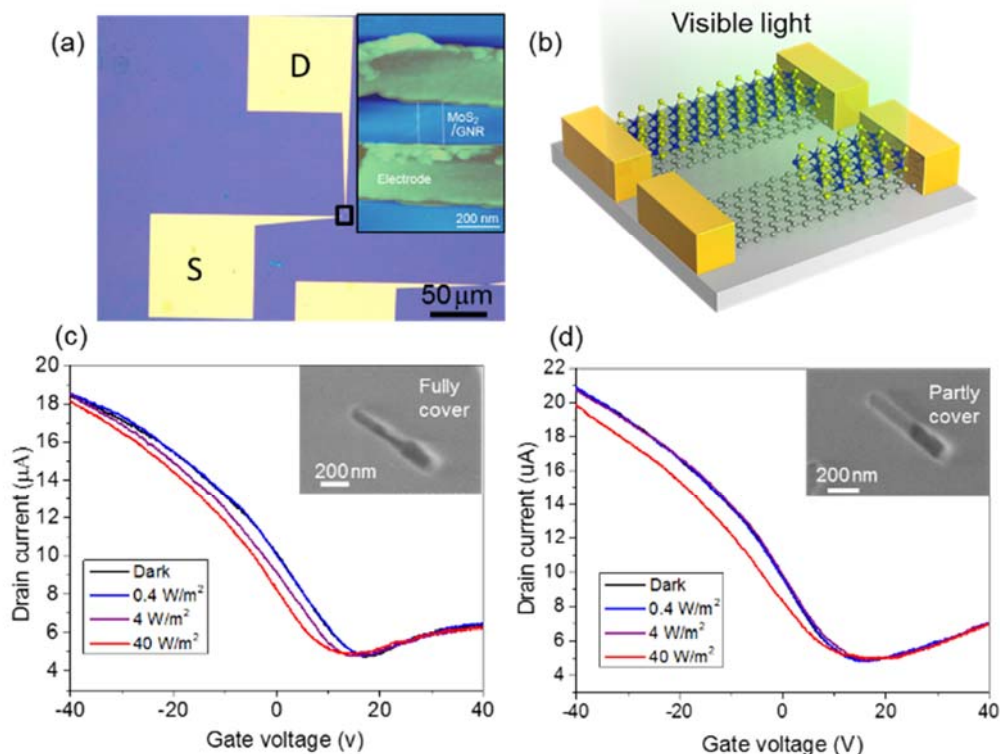


Fig. 4 (a) Optical microscope image of a FET having MoS₂/GNR as a channel. Inset shows an AFM image of the channel. (b) Schematic diagram of the FET for fully and partially covered MoS₂ on GNR with visible light illumination. (c) Transfer curves of fully covered MoS₂/GNR device measured in dark and under illumination with different power densities ($V_d = 0.1V$). Inset shows a SEM image of fully covered MoS₂ on GNR, taken before making devices, which is the identical sample used to measure the transfer curve. (d) Partly covered MoS₂/GNR device data.

Using the MoS₂/GNR heterostructures, we fabricated back-gated MoS₂/GNR transistors for both fully and partly covered samples. The electrode patterns (Au(40 nm)/Ti(5 nm)) were made by EB lithography, EB metal evaporation, and lift-off processes. The typical channel length was designed to be 200 nm ~ 1 µm depending on the GNR length. Black curves in Figure 4c,d represent the transfer characteristics of the GNR devices fully (Fig. 4c) and partly covered with MoS₂ (Fig. 4d) measured in dark. Both devices showed ambipolar behavior with enhanced p-type conduction, which is widely observed for graphene FETs,³⁷ thus we consider that the carrier transport is dominated by GNR which has higher conductivity than MoS₂. As we widely observed p-type characteristic for graphene FETs even without MoS₂,³⁷ the origin of p-type can be originated in the unintentional doping from contamination, lithography processes, and/or surface adsorbates.

The two-terminal field-effect mobility in the dark was calculated to be 1,000 and 1,200 cm²/Vs for fully and partly covered MoS₂/GNR devices, respectively. As we already mentioned that there is no boundary in a single GNR,²¹ the carrier mobility is relatively high in spite of a very narrow GNR channel width and the second CVD growth of the MoS₂ layer.

Graphene is almost transparent to the visible light due to very low optical absorption coefficient (2.3%)¹ and, therefore, graphene transistors are generally insensitive to the optical light. However, by integrating with MoS₂ which has strong optical absorption (1×10^7 m⁻¹) and 1.9 eV band gap,⁹ we can expect high sensitivity to visible light, acting as a high gain photodetector. Therefore, we measured the transport properties under a laser illumination with 532 nm, as illustrated in Figure 4b. We clearly

observed the photo-induced current modulation for both fully covered and partly covered devices (Fig. 4c,d). Three filters with different optical densities (OD) were used to change the incident laser power (OD1: 40 W/m², OD2: 4 W/m² and, OD3: 0.4 W/m²), and the highest laser power (OD1) gave the clearest response. The drain current was found to decrease at gate voltage (V_g) below Dirac point (V_D), while the current slightly increased when $V_g > V_D$. This can be explained by the photo-induced electron transfer from MoS₂ to GNR; the main carrier is holes for $V_g < V_D$ so that the electron transferred from MoS₂ reduced the current, while electron carriers slightly increased for $V_g > V_D$ (but not significantly because of the band levels).³⁶ The modulation of the drain current by the visible light was as high as 16~17%, under ~40 W/m² for both devices. We note that this value is much higher than that reported for the large MoS₂/graphene heterostructure (2%) illuminated with the higher intensity laser (140 W/m²).³⁶ Because the channel sizes of the present MoS₂/GNR devices are relatively small, these devices act under low illumination suggesting high-gain photodetector. The fact that our MoS₂/GNR heterostructure showed much higher photo-sensitivity than planar MoS₂/graphene, suggests that charge separation (photo-induced electron transfer) is more enhanced by GNR than large-area graphene. The modulation of graphene's band structure due to GNR structure and/or significant effect of graphene edge might be the reason for the observed sensitivity, but further study is necessary to understand the mechanism of charge separation in the MoS₂-GNR systems.

Conclusions

We demonstrate the direct growth of vertical MoS₂/GNR heterostructures by two-step CVD using oriented GNRs grown on the epitaxial Cu(100) film. We found that the MoS₂ grows preferentially on GNRs, while no MoS₂ formation is observed on a SiO₂ substrate. The formation of the MoS₂/GNR heterostructures was confirmed by AFM, SEM, Raman, and TEM-EDX measurements. Moreover, through the control of the CVD condition, we can synthesize the heterostructures with different MoS₂ coverage, including partially covered MoS₂/GNR heterostructure. We also demonstrated that the current modulation by visible light is much more enhanced for our MoS₂/GNR system when compared with a planar MoS₂/graphene system. Our findings are expected to offer a new route to grow heterostructures with controlled dimensionality and can be applied to electronic and photonic devices through the combination of different components of layered materials.

Acknowledgements

This work was supported by the PRESTO-JST and KAKENHI (15H03530, 15K13304). RMY acknowledges the receipt of scholarship from MARA, Malaysia. We thank Prof. Dr. Shiyoshi Yokoyama for the kind assistance of EB lithography.

References

- 1 A. K. Geim, *Science*, 2009, **324**, 1530–1534.
- 2 K. S. Novoselov, V. I. Fal'ko, L. Colombo, P. R. Gellert, M. G. Schwab and K. Kim, *Nature*, 2012, **490**, 192–200.
- 3 A. D. Yoffe, *Solid State Ion.*, 1990, **39**, 1–7.
- 4 Q. H. Wang, K. Kalantar-Zadeh, A. Kis, J. N. Coleman and M. S. Strano, *Nat. Nanotechnol.*, 2012, **7**, 699–712.
- 5 C. R. Dean, A. F. Young, I. Meric, C. Lee, L. Wang, S. Sorgenfrei, K. Watanabe, T. Taniguchi, P. Kim, K. L. Shepard and J. Hone, *Nat. Nanotechnol.*, 2010, **5**, 722–726.
- 6 L. Li, Y. Yu, G. J. Ye, Q. Ge, X. Ou, H. Wu, D. Feng, X. H. Chen and Y. Zhang, *Nat. Nanotechnol.*, 2014, **9**, 372–377.
- 7 H. Lim, S. I. Yoon, G. Kim, A.-R. Jang and H. S. Shin, *Chem. Mater.*, 2014, **26**, 4891–4903.
- 8 K. S. Novoselov, A. K. Geim, S. V. Morozov, D. Jiang, Y. Zhang, S. V. Dubonos, I. V. Grigorieva and A. A. Firsov, *Science*, 2004, **306**, 666–669.
- 9 K. F. Mak, C. Lee, J. Hone, J. Shan and T. F. Heinz, *Phys. Rev. Lett.*, 2010, **105**, 136805.
- 10 K. S. Novoselov, D. Jiang, F. Schedin, T. J. Booth, V. V. Khotkevich, S. V. Morozov and A. K. Geim, *Proc. Natl. Acad. Sci. U. S. A.*, 2005, **102**, 10451–10453.
- 11 W. Zhang, C.-P. Chuu, J.-K. Huang, C.-H. Chen, M.-L. Tsai, Y.-H. Chang, C.-T. Liang, Y.-Z. Chen, Y.-L. Chueh, J.-H. He, M.-Y. Chou and L.-J. Li, *Sci. Rep.*, 2014, **4**.
- 12 K. Roy, M. Padmanabhan, S. Goswami, T. P. Sai, G. Ramalingam, S. Raghavan and A. Ghosh, *Nat. Nanotechnol.*, 2013, **8**, 826–830.
- 13 W. J. Yu, Y. Liu, H. Zhou, A. Yin, Z. Li, Y. Huang and X. Duan, *Nat. Nanotechnol.*, 2013, **8**, 952–958.
- 14 S. Bertolazzi, D. Krasnozhan and A. Kis, *ACS Nano*, 2013, **7**, 3246–3252.
- 15 X. Li, X. Wang, L. Zhang, S. Lee and H. Dai, *Science*, 2008, **319**, 1229–1232.
- 16 M. Y. Han, B. Özyilmaz, Y. Zhang and P. Kim, *Phys. Rev. Lett.*, 2007, **98**, 206805.
- 17 Y.-W. Son, M. L. Cohen and S. G. Louie, *Phys. Rev. Lett.*, 2006, **97**, 216803.
- 18 V. Barone, O. Hod and G. E. Scuseria, *Nano Lett.*, 2006, **6**, 2748–2754.
- 19 M. Wimmer, İ. Adagideli, S. Berber, D. Tománek and K. Richter, *Phys. Rev. Lett.*, 2008, **100**, 177207.
- 20 Y. Li, Z. Zhou, S. Zhang and Z. Chen, *J. Am. Chem. Soc.*, 2008, **130**, 16739–16744.
- 21 R. Mohamad Yunus, M. Miyashita, M. Tsuji, H. Hibino and H. Ago, *Chem. Mater.*, 2014, **26**, 5215–5222.
- 22 G. W. Shim, K. Yoo, S.-B. Seo, J. Shin, D. Y. Jung, I.-S. Kang, C. W. Ahn, B. J. Cho and S.-Y. Choi, *ACS Nano*, 2014, **8**, 6655–6662.
- 23 Y. Shi, W. Zhou, A.-Y. Lu, W. Fang, Y.-H. Lee, A. L. Hsu, S. M. Kim, K. K. Kim, H. Y. Yang, L.-J. Li, J.-C. Idrobo and J. Kong, *Nano Lett.*, 2012, **12**, 2784–2791.
- 24 X. Ling, Y.-H. Lee, Y. Lin, W. Fang, L. Yu, M. S. Dresselhaus and J. Kong, *Nano Lett.*, 2014, **14**, 464–472.
- 25 A. Azizi, S. Eichfeld, G. Geschwind, K. Zhang, B. Jiang, D. Mukherjee, L. Hossain, A. F. Piasecki, B. Kabius, J. A. Robinson and N. Alem, *ACS Nano*, 2015, **9**, 4882–4890.
- 26 L. M. Malard, M. A. Pimenta, G. Dresselhaus and M. S. Dresselhaus, *Phys. Rep.*, 2009, **473**, 51–87.

- 27 C. Casiraghi, A. Hartschuh, H. Qian, S. Pisanec, C. Georgi, A. Fasoli, K. S. Novoselov, D. M. Basko and A. C. Ferrari, *Nano Lett.* 2009, **9**, 1433–1441.
- 28 B. C. Windom, W. G. Sawyer and D. W. Hahn, *Tribol. Lett.*, 2011, **42**, 301–310.
- 29 H. Li, Q. Zhang, C. C. R. Yap, B. K. Tay, T. H. T. Edwin, A. Olivier and D. Baillargeat, *Adv. Funct. Mater.*, 2012, **22**, 1385–1390.
- 30 D. J. Late, B. Liu, H. S. S. R. Matte, C. N. R. Rao and V. P. Dravid, *Adv. Funct. Mater.*, 2012, **22**, 1894–1905.
- 31 C. Lee, H. Yan, L. E. Brus, T. F. Heinz, J. Hone and S. Ryu, *ACS Nano*, 2010, **4**, 2695–2700.
- 32 A. Splendiani, L. Sun, Y. Zhang, T. Li, J. Kim, C.-Y. Chim, G. Galli and F. Wang, *Nano Lett.*, 2010, **10**, 1271–1275.
- 33 D. V. Kosynkin, A. L. Higginbotham, A. Sinitskii, J. R. Lomeda, A. Dimiev, B. K. Price and J. M. Tour, *Nature*, 2009, **458**, 872–876.
- 34 S. Ryu, J. Maultzsch, M. Y. Han, P. Kim and L. E. Brus, *ACS Nano*, 2011, **5**, 4123–4130.
- 35 X. Wang and H. Dai, *Nat. Chem.*, 2010, **2**, 661–665.
- 36 H. Ago, H. Endo, P. Solís-Fernández, R. Takizawa, Y. Ohta, Y. Fujita, K. Yamamoto and M. Tsuji, *ACS Appl. Mater. Interfaces*, 2015, **7**, 5265–5273.
- 37 H. Ago, K. Kawahara, Y. Ogawa, S. Tanoue, M. A. Bissett, M. Tsuji, H. Sakaguchi, R. J. Koch, F. Fromm, T. Seyller, K. Komatsu and K. Tsukagoshi, *Appl. Phys. Express*, 2013, **6**, 075101.